Sensors & Diagnostics

ROYAL SOCIETY OF CHEMISTRY

COMMUNICATION

View Article Online
View Journal | View Issue

Cite this: *Sens. Diagn.*, 2022, **1**, 968

Received 6th April 2022,
Accepted 26th July 2022

DOI: 10.1039/d2sd00067a

rsc.li/sensors

Development of a label-free electrochemiluminescence biosensor for the sensitive detection of porcine gelatin using carbon nanostructured materials

Juthi Adhikari, [a] Mohammad Rizwan [b] and Minhaz Uddin Ahmed *[a]

In this study, a carbon nanofiber fabricated screen-printed electrode (CNF-SPE) was modified using carbon nano-horns (CNHs) and nafion (NAF) for the development of a label-free electrochemiluminescence (ECL) biosensor. The goal was to design a robust and sensitive biosensor for the detection of porcine gelatin in food products, which will globally have a significant impact on the halal food industry. Gelatin derived from porcine has major religious and ethical concerns worldwide and its use is gradually increasing in food-based products without proper monitoring and observation. Henceforth, a biosensor was developed over a CNFs-SPE/CNHs/NAF platform by immobilizing biorecognition molecules (anti-gelatin), followed by non-specific blocking by 0.1% bovine serum albumin (BSA). Further, energy dispersive X-ray (EDX) and Fourier-transform infrared (FTIR) spectroscopy were employed to characterize the CNHs/NAF nanocomposite. Moreover, biosensor development was studied both by ECL and electrochemical impedance spectroscopy. Interestingly, the developed biosensor CNFs-SPE/CNHs/NAF/anti-gelatin/BSA demonstrated extensive linearity of 1 pg mL^{-1} to 8 ng mL^{-1} with a detection limit of 1 pg mL^{-1}. Therefore, with a demonstrated wide linear range and low detection limit, this proposed biosensor could be used to analyze real food samples. Furthermore, the biosensor showed remarkable reproducibility for porcine gelatin detection.

1. Introduction

Gelatin is a translucent, colorless protein extracted from collagen, which can be abundantly found in animal skin, cartilage, and bones.[1] Gelatin has been in high demand in different industries for various applications. A few important examples of gelatin-demanding industries include food, pharmaceutical, and cosmetics, as well as sectors producing photographic films and paper.[2] Moreover, the sources of gelatin include porcine, bovine, chicken, fish, and donkey.[3] Therefore, the acceptability of gelatin highly depends on its sources.[4] However, the usage of gelatin in food such as trifles, candy corn, and gummy bears isolated from porcine and bovine has major religious and ethical concerns across the globe, especially among Muslims and Jews.[5,6] Further, the current trend of practicing vegetarian and vegan lifestyles does not support the use of gelatin in different products from animal sources.[7]

Whilst ELISA,[8] chromatography,[9] mass spectroscopy,[10] infrared-spectroscopy,[11] and PCR-based methods are currently available to detect gelatin.[12] However, each method has its limitation including low sensitivity, low specificity, tedious, time-intensive, expensive, confinement, bulky instrumentations, and the requirement of a trained person. Moreover, none of these methods demonstrate the potential to detect traces of porcine gelatin. Therefore, a highly sensitive, highly specific, rapid, robust, inexpensive, portable method with the potential to be used as an on-site testing device is urgently required. Therefore, in this study, a label-free electrochemiluminescence (ECL) biosensor over a carbon nano-fiber screen-printed electrode (CNF-SPE) for the sensitive detection of gelatin using nanostructured carbon materials has been proposed.

Currently, different carbon nanostructured materials (CNSMs) are being employed in developing biosensors for the sensitive detection of target proteins.[13] The integration of different CNSMs in developing biosensors has attained notable acceptability since the last decade[14] as they provide rapid and continuous signal measurement,[15] high sensitivity, high specificity with quick response time,[16,17] and require fewer reagents and solution.[18] For example, carbon nano-horns (CNHs) and carbon nano-fibers (CNFs) have attracted significant attention from researchers and scientists in biosensing applications due to their novel properties.[19,20]

[a] *Biosensors and Nanobiotechnology Laboratory, Chemical Sciences, Faculty of Science, Universiti Brunei Darussalam, Jalan Tungku Link, Gadong, BE1410, Brunei Darussalam. E-mail: minhaz.ahmed@ubd.edu.bn*
[b] *Electrochemistry@Soft Interfaces (E@SI) Group, Department of Inorganic and Analytical Chemistry, Faculty of Chemistry, University of Lodz, Tamka 12, 91-403 Lodz, Poland*

CNHs are conically shaped, one-dimensional (1-D) CNSMs, having high surface area, high electrochemical conductivity, exceptional porosity, and remarkable catalytic properties.[21] Further, CNFs have a large electrochemical surface area and high electronic conductivity.[22] Moreover, a $[Ru(bpy)_3]^{2+}$/TPrA system has demonstrated excellent ECL signal over a CNF-based electrode.[23]

In recent years, the ECL technique has obtained remarkable attention in the development of biosensors due to its versatility and stability.[24,25] Moreover, the incorporation of different carbon-based nanomaterials has also aided the trend of using ECL methods in developing nano-biosensors.[26,27] The core mechanism of an ECL-based biosensor depends on the interaction between the luminophore and the target protein or antigen.[28] Hence, it is extremely important to use a reliable luminophore and co-reactant mixture to ensure stable and reproducible ECL signals, which get amplified by nanostructured materials.[29,30] Thus, in this study, we have selected tris(2,2′-bipyridyl) dichlororuthenium(II) hexahydrate $[Ru(bpy)_3]Cl_26H_2O$ as the luminophore and tripropylamine (TprA) as the co-reactant.

Screen-printed electrodes offer reproducibility, miniaturization, portability, and affordability with a high potential for mass-production.[31,32] Therefore, we have proposed an ECL biosensor for the sensitive detection of gelatin (gltn) over CNF-SPE modified with CNHs and Nafion (NAF). In addition, to be a binder, NAF provides chemical stability as well as good antifouling capacity.[33] Moreover, the proposed CNFs-SPE/CNHs/NAF/anti-gltn/BSA biosensor displayed a remarkable linear range of 1 pg mL^{-1} to 8 ng mL^{-1} with a low detection limit of 1 pg mL^{-1} to detect porcine gelatin. Further, the CNFs-SPE/CNHs/NAF/anti-gltn/BSA biosensor demonstrated high reproducibility in detecting porcine gelatin.

2. Materials and methods

2.1 Reagents

Anti-porcine gelatin (anti-gltn) and porcine gelatin protein (gltn) were procured from Alpha Diagnostics International (Texas, USA). Bovine serum albumin (BSA), sodium azide (NaN_3), potassium chloride (KCL), potassium ferrocyanide ($K_4[Fe(CN)_6]$), potassium ferricyanide ($K_3[Fe(CN)_6]$), carbon nanohorns, carbon nano chips, mesoporous carbon, $[Ru(bpy)_3]Cl_26H_2O$, TprA (98% purity), tris, disodium phosphate, and monosodium phosphate were purchased from Sigma-Aldrich (Saint Louis, USA). Carbon nano-onions were purchased from carbon allotropes (Kensington, Australia), binding agent, Nafion was purchased from Alfa Aesar (Ward Hill, M.A.). For all the analysis, samples were diluted using 10 mM PBS (pH 7.4). All chemicals and reagents were of ≥95% purity. All reagents and solutions were prepared utilizing freshly obtained Milli-Q water (deionized with a specific resistance of ~18 M cm^{-1}). Each of these analyses was done at least three times (n = 3), and the average was presented with a standard deviation. All the experiments were done at a constant room temperature of 20 ± 0.5 °C.

2.2 Apparatus

ECL measurements were done using an MPI-A capillary electrophoresis ECL analyzer system, which was bought from Xi'an Yima Opto-Electrical Technology Co., Ltd. (China). An in-house ECL cell was prepared to measure the light produced from the reactions between the luminophore and the coreactant at the working electrode. The ECL cell was placed over the photomultiplier tube (PMT) attached to the MPI-A software to determine ECL intensity. All the ECL measurements were performed using equal volume (1 mL each) of 100 mM $[Ru(bpy)_3]Cl_2$ solution and 1 mM TPrA solution, and the total volume of cell was maintained at 4 mL using 10 mM PBS pH 7.4. The electrochemical impedance spectroscopy study was performed using Autolab PGSTAT101 III potentiostat/galvanostat (Metrohm, Netherlands) connected to a Nova software version 1.10. The carbon nano-fiber screen printed electrodes were procured from DropSens (Spain), where the reference electrode was silver coated, and the counter electrode was coated with carbon. The diameter of the working electrode was 4 mm with a maximum working volume of 50 μL. Nanocomposite characterization was performed using both Fourier-transform infrared (FTIR) spectroscopy attached with a MIRacle single-reflection attenuated total reflectance (ATR) (Shimadzu, Japan), and energy dispersive X-ray (EDX) (Tokyo, Japan). All the experiments were performed in an air-conditioned laboratory having a constant temperature of 20 ± 0.5 °C.

2.3 Preparation of the nanocomposite

The preparation of the selected CNHs/NAF nanocomposite was accomplished in-house at RT at 20 ± 0.5 °C. In brief, for the preparation of the CNHs/NAF nanocomposite, 0.5 mg of CNHs were dispersed in 1 mL of autoclaved-distilled water. To ensure the proper dispersion of the nanoparticle, it was sonicated using an ultra-sonicator for 2.5 h. Following that, a 0.1% NAF solution was prepared by serially diluting it from the original stock (5%) using 0.01 M PBS solution (pH 7.4). Finally, for the synthesis of the final nanocomposite, 0.5 mg mL^{-1} of the CNH solution was mixed with the 0.1% NAF solution at a 2 : 1 ratio and was mixed using a magnetic stirrer for 5 h for proper dispersion. This in-house prepared nanocomposite can be stored at 4 °C for further use. In addition, before each use, the nanocomposite mixture was sonicated for 30 min.

2.4 Fabrication of the porcine gelatin biosensor

Before the ECL signal determination, the CNFs-SPE working electrode was incubated using 10 μL of the CNHs/NAF nanocomposite and dried at RT. Following that, the electrode was washed using 10 μL PBS solutions (10 mM). Then, 20 μL of biorecognition molecules (anti-gelatin, 10 μg mL^{-1}) was immobilized over a nanocomposite modified electrode and

incubated overnight. The excess biorecognition molecules were thoroughly washed using 10 μL of PBS buffer. This step was followed by 45 min incubation with a 0.1% BSA solution as a blocking agent to prevent any non-specific binding sites on the fabricated electrode. Finally, the CNFs-SPE/CNHs/NAF/anti-gltn/BSA biosensor was washed with 10 mM of PBS buffer and used for ECL measurement or stored until the next use at 4 °C. Biosensor fabricating and ECL signal determination is illustrated in Scheme 1.

2.5 Electrochemiluminescence signal measurement

In order to determine the ECL signal, different concentrations of the porcine gelatin were incubated over the CNFs-SPE/CNHs/NAF/anti-gltn/BSA biosensor for 60 min. Next, the immunosensor incubated with gelatin (CNFs-SPEs/CNHs/NAF/anti-gltn/BSA/gltn) was washed with the PBS solution to remove any loosely bound or unbound porcine gelatin from the surface of the biosensor and dried at RT. Following, ECL readings in the cyclic voltammetric mode were obtained at PMT tube voltage 800 V at the scan rate 100 mV s^{-1}. The sensitivity and amplifying series were also kept constant to minimize the background signal. The average peak currents of each concentration were then analyzed and calculated.

3. Results and discussion

3.1 Selection of carbon nanostructured materials

For the selection of the suitable carbon-based nanomaterial to modify CNFs-SPE, we tested different types of CNSMs and NAF composite: CNHs, carbon nanochips (CNCs), mesoporous carbon (MC), and carbon nano-onions (CNOs). Among them, CNHs showed the maximum ECL signal (Fig. 1A). This may be due to one dimensional (1-D) conically shaped CNHs having a high surface area, high electrochemical conductivity, exceptional porosity, and remarkable catalytic properties,[21] which enable them to give stable ECL intensity over the CNF electrode.[22] Moreover, the production of ECL occurs followed by the application of a voltage at the fabricated electrode, which leads to a redox reaction between the luminophore ($[Ru(bpy)_3]Cl_26H_2O$) and the co-reactant (TprA) over the electrode surface. The redox reaction results in the formation of an excited state of the luminophore (Ru^{2+}*), which relaxes to the ground state and generates light at λ = ~620 nm.[31] This generated light is recorded as an ECL signal.[16]

Further, in order to figure out the suitable and reproducible working ratio between the selected nanomaterial (CNHs) and binder (NAF), we studied multiple probable ratios (*i.e.*, 1 : 2, 2 : 1, and 1 : 3). Interestingly, the 2 : 1 ratio of CNHs and NAF showed the highest ECL intensity over CNFs-SPE, which was chosen for further study (Fig. 1B). Furthermore, before selecting a working ratio between any carbon-based nanomaterial and binder, first, we need to evaluate that the binder is not interfering with the signal of the selected nanomaterial performing any electrochemical analysis such as ECL and electrochemical impedance spectroscopy (EIS). Moreover, the main reason for choosing nafion with CNHs was it provided stable, consistent, and reproducible data in different experiments. In addition, the ratio of 2 : 1 showed maximum ECL intensity compared to a blank or bare electrode (CNFs-SPE). Therefore, the ratio between CNHs and NAF of 2 : 1 was selected for further study. Possibly, the stable electrochemical property of nafion played a vital role in maintaining consistent and repeatable results.[33]

3.2 EDX and FTIR characterization of the CNHs/NAF nanocomposite

Both EDX and FTIR characterizations were employed for the assessment of the successful formation of the CNHs/NAF nanocomposite. CNHs and the CNHs/NAF nanocomposite were spiked over 1 cm glass slides and dried overnight for EDX characterization studies. Fig. 2A shows the highest peak of carbon with a 33.27 elemental percentage. Moreover, sharp peaks of fluorine (F) and sulfur (S) were observed (Fig. 2B) in addition to the carbon peak when the CNHs/NAF nanocomposite was studied. This study proved the successful formation of the CNHs/NAF nanocomposite.

Fig. 3 shows the FTIR results of the CNHs/NAF nanocomposite study. In the case of CNHs [Fig. 3 curve (a)],

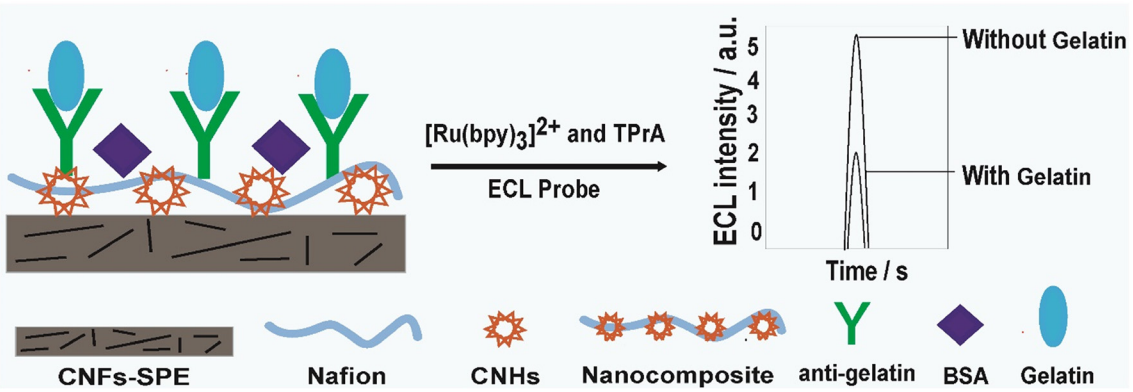

Scheme 1 Biosensor fabrication and ECL signal determination.

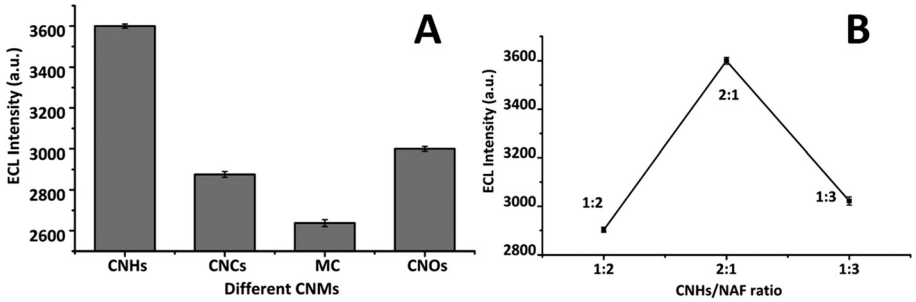

Fig. 1 (A) Selection of the carbon nanostructured materials; and (B) selection of the CNHs and NAF ratio for the CNHs/NAF nanocomposite.

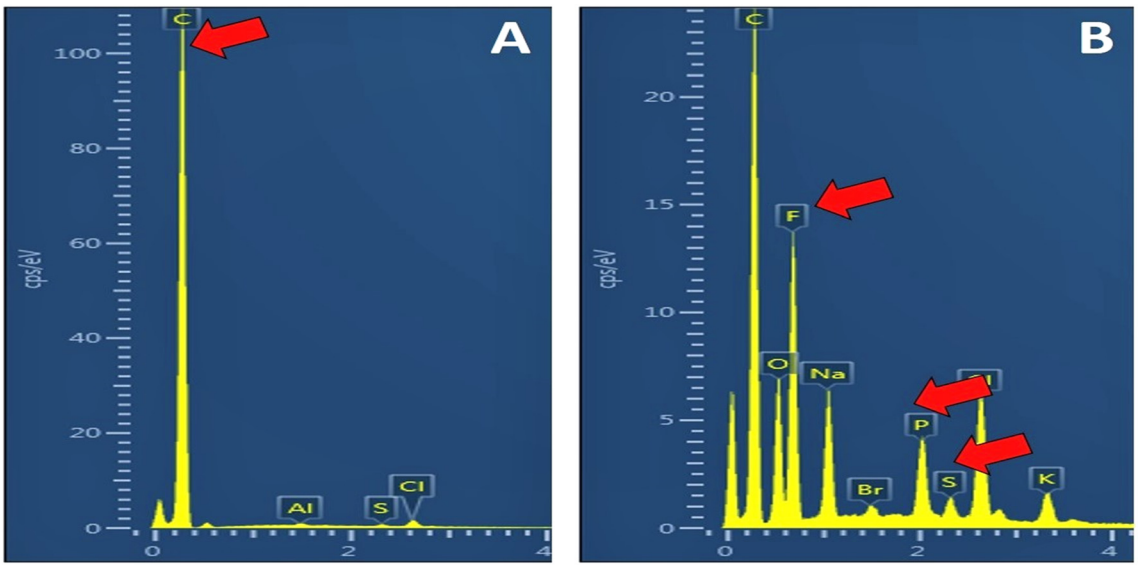

Fig. 2 EDX characterization of the CNHs/NAF nanocomposite (A) CNHs; and (B) CNHs/NAF.

the most prominent peaks were observed in two separate regions 700 to 1600 cm^{-1} and 2900 to 3400 cm^{-1}. Besides, the peak at 3410.29 cm^{-1} signifies the –OH stretching, and the peak at 2924.21 cm^{-1} shows the symmetric and anti-symmetric alignments of the C–H groups.[35] In addition, the peaks at 1613.52 cm^{-1} and 1219.06 cm^{-1} denoted the SP^2 hybridized aromatic carbon (C=C) and C–O stretching vibrations, respectively.[36] For the CNHs/NAF nanocomposite, the major FTIR spectra was observed at 600 to 1600 cm^{-1} and 2800 to 3400 cm^{-1} regions [Fig. 3 curve (b)].The peak at 3431.51 cm^{-1} showed the bending vibrations of water molecules (–OH) stretching.[37] In addition, the peak at 1641.49 cm^{-1} indicated the O–H bending vibrations,[38] and peaks at 1235.46 cm^{-1} and 1053.18 cm^{-1} denoted the asymmetric CF_2 stretching and symmetric S–O bending

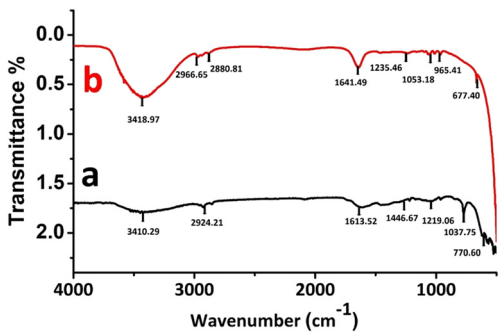

Fig. 3 FTIR characterization of the CNHs/NAF nanocomposite (a) CNH and (b) CNHs/NAF.

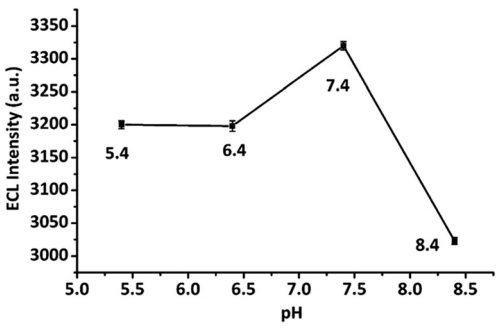

Fig. 4 pH evaluation of the reaction medium.

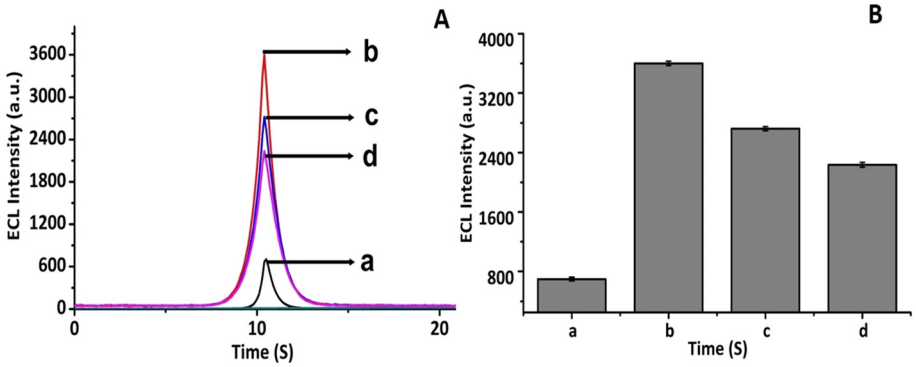

Fig. 5 ECL study of the CNFs-SPE/CNHs/NAF/anti-gelatin/BSA immunosensor (A) ECL curves; and (B) bar of the ECL peak, where: (a) bare CNFs-SPE, (b) CNFs-SPE/CNHs/NAF, (c) CNFs-SPE/CNHs/NAF/ant-gltn, and (d) CNFs-SPE/CNHs/NAF/ant-gltn/BSA.

vibrations, respectively. Moreover, the peak at 965.41 cm^{-1} indicated the symmetric C–O–C alignments.[39] Thus, the FTIR spectra further confirmed the successful formation of the CNHs/NAF nanocomposite.

3.3 pH evaluation of the reaction medium

The ionic strength of the medium influences the sensing signal. Therefore, a medium of 10 mM PBS having optimum ionic strength for sensing application has been used following standard references.[23,34] Moreover, to confirm the optimum pH for the ECL signal of the biosensor, different pH ranges (5.4, 6.4, 7.4, and 8.4) were tested. The biosensor demonstrated the highest and stable ECL signal with 10 mM PBS solution of pH 7.4 (Fig. 4). Therefore, 10 mM PBS solution of pH 7.4 was used throughout the study.

3.4 ECL characterization of CNFs-SPE/CNHs/NAF/anti-gltn/BSA

To perform the layer-by-layer ECL characterization of the CNFs-SPE/CNHs/NAF/anti-gltn/BSA biosensor, each layer was separately studied and data was recorded. At first, the ECL signal of the bare CNFs-SPE was recorded [Fig. 5A curve (a)]. Next, the bare CNFs-SPE was incubated with the CNHs/NAF composite and dried for 2 h, followed by measuring the ECL signal. It was found that the ECL intensity of the CNHs/NAF layer was much higher compared to that of the bare CNFs-SPE [Fig. 5A curve (b)]. This may be due to the high electrochemical conductivity of the CNHs facilitating electron transfer between the ECL probe and the working electrode. Later, the CNHs/NAF modified electrode (CNFs-SPE/CNHs/NAF) was further incubated with biorecognition molecules (anti-gltn), followed by blocking with 0.1% BSA to inhibit the non-specific binding sites. The incubation of biorecognition molecules showed a decrease in the intensity of the ECL signal due to the formation of an insulating layer (CNFs-SPE/CNHs/NAF/anti-gltn) over the CNFs-SPE/CNHs/NAF surface [Fig. 5A curve (c)]. Similarly, the introduction of BSA further decreased the intensity of the ECL signal [Fig. 5A, curve (d)] confirming the formation of an additional insulating layer (CNFs-SPE/CNHs/NAF/anti-gltn/BSA) and successful formation of the immunosensor for the detection of gelatin. Fig. 5A bar (a)–(d) show the peak of the ECL intensity of bare CNFs-SPE, CNFs-SPE/CNHs/NAF, CNFs-SPE/CNHs/NAF/anti-gltn and CNFs-SPE/CNHs/NAF/anti-gltn/BSA.

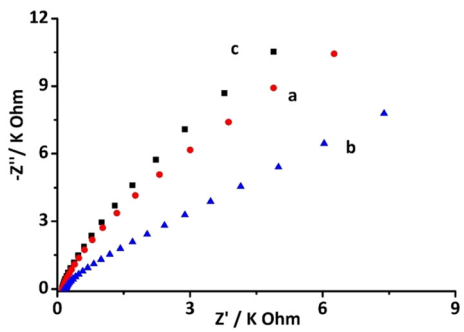

Fig. 6 EIS characterization of the CNFs-SPE/CNHs/NAF/anti-gltn/BSA biosensor, where: (a) bare CNFs-SPE, (b) CNFs-SPE/CNHs/NAF and (c) CNFs-SPE/CNHs/NAF/ant-gltn/BSA [5 mM $K_3[Fe(CN)_6]/K_4[Fe(CN)_6$, 0.1–100 kHz, ac amplitude 10 mV and number of frequency 50 Hz].

3.5 EIS study CNFs-SPE/CNHs/NAF/anti-gltn/BSA

In addition, electrochemical impedance spectroscopy (EIS) was also employed for the characterization of biosensor formation. The EIS data showcased semicircular patterns along with some straight-line sections, which signified the charge transfer resistance (R_{ct}) and diffusion-controlled processes. According to the Nyquist theory, the charge transfer resistance (R_{ct}) of the incubated layer is directly related to the diameter of the semicircle.[40,41] Fig. 6 shows the EIS pattern of different layers of the fabricated CNFs-SPE/CNHs/anti-gltn/BSA biosensor. Fig. 6 curve (a) depicts the EIS signal of bare CNFs-SPE, whilst Fig. 6 curve (b) depicts the EIS signal of CNFs-SPE/CNHs/NAF. CNFs-SPE demonstrated a higher EIS signal compared to CNFs-SPE/CNHs/NAF. This is attributable to the fact that CNHs provide high electrochemical conductivity resulting in lower resistance than the bare CNFs-SPE. However, Fig. 6 curve (c) shows the EIS signal of CNFs-SPE/CNHs/NAF incubated both with

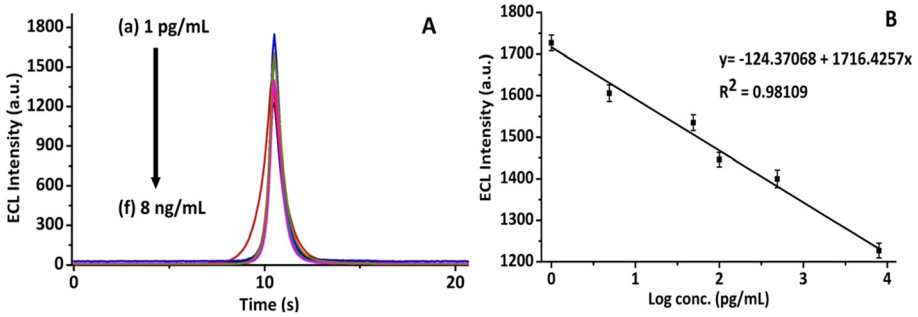

Fig. 7 Analytical performance study of the proposed biosensor (A) concentration dependent line graph from 1 pg mL^{-1} to 8 ng mL^{-1}: (a) 1 pg mL^{-1}, (b) 5 pg mL^{-1}, (c) 50 pg mL^{-1}, (d) 100 pg mL^{-1}, (e) 500 pg mL^{-1}, (f) 8 ng mL^{-1}; (B) the calibration plot from 1 pg mL^{-1} to 8 ng mL^{-1} of porcine gelatin.

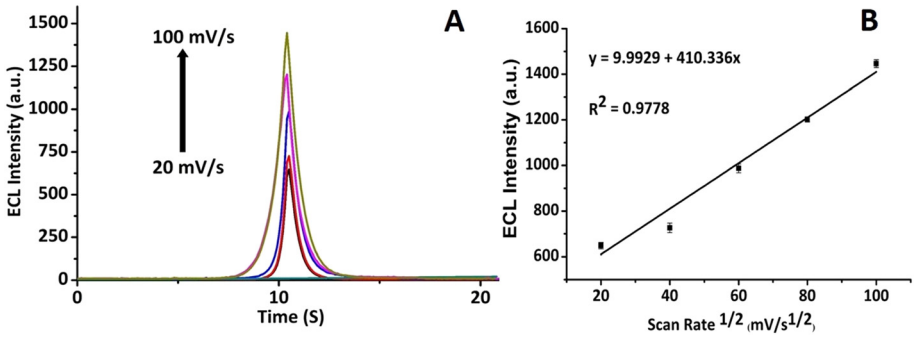

Fig. 8 Diffusion kinetic study of the biosensor assessed by the ECL intensity. (A) ECL intensity of the developed immunosensor from 20 mV s^{-1} to 100 mV s^{-1} at an interval of 20; and (B) relationship between the peak value of the ECL intensity and the square root of scan rates.

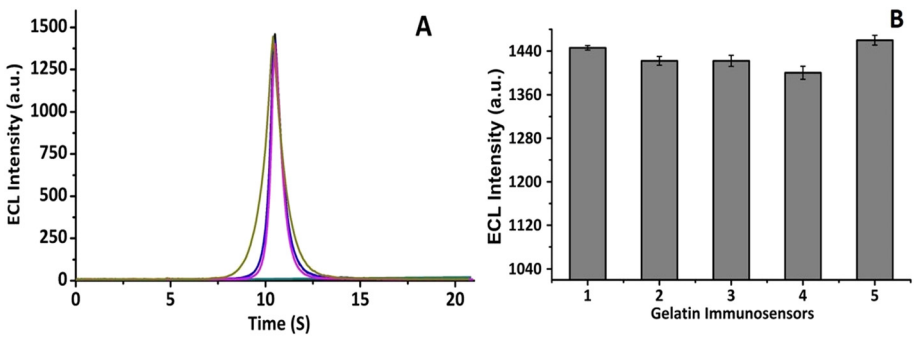

Fig. 9 Reproducibility study of CNFs-SPE/CNHs/NAF/anti-gltn/BSA biosensors incubated with 100 pg mL^{-1} porcine gelatin: (A) ECL intensity graph of five biosensors; and (B) corresponding ECL intensity peak bar graph.

biorecognition molecules (anti-gltn) and BSA. The CNFs-SPE/CNHs/anti-gltn/BSA biosensor showed an increase in the EIS signal due to high resistance by the insulating layer of biorecognition molecules and blocking agent. Indeed, the EIS further confirms the formation of the CNFs-SPE/CNHs/NAF/anti-gltn/BSA biosensor.

3.6 Analytical performance of the biosensor

The analytical performance of the proposed CNFs-SPE/CNHs/NAF/anti-gltn/BSA biosensor was evaluated by testing different concentrations of gelatin from 1 pg mL^{-1} to 8 ng mL^{-1}. Fig. 7A shows the concentration-dependent graph of the biosensor to detect porcine gelatin. Fig. 7B shows the calibration plot between logarithmic concentrations of porcine gelatin and ECL intensity. With the increase in the concentration of the porcine gelatin, the ECL intensity correspondingly decreased. This could be attributed to the insulating nature of porcine gelatin that inhibits electron transfer between the ECL probe and the working electrode surface.[34,42] Thus, up to saturation concentration (8 ng mL^{-1}), the biosensor responded to bind porcine gelatin, and correspondingly the ECL intensity decreased.[43] Further, this evaluated concentration range is acceptable for detecting gelatin in food.[44] Moreover, the proposed biosensor was experimentally demonstrated to detect the lowest concentration of 1 pg mL^{-1} of gelatin.[23,34] This low limit of detection of the immunosensor could be due to the

synergistic electrochemical conductive properties provided by both CNFs and CNHs.[21,22]

3.7 Label-free detection principle

ECL scan rate study of the CNFs-SPE/CNHs/NAF/anti-gltn/BSA biosensor incubated with gelatin was performed to evaluate the electrochemical diffusion control process. The ECL scan rate study showed an increase in the ECL signal with an increase in the scan rate (Fig. 8A). Further, a linear relationship between the peak value of the ECL intensity and the square root of scan rates was observed with an "*R*" value of 0.9778 (Fig. 8B). This established that the developed CNFs-SPE/CNHs/NAF/anti-gltn/BSA biosensor followed electrochemical diffusion control kinetics for the detection of porcine gelatin.[23,34]

3.8 Reproducibility performance

To evaluate the reproducibility performance, five CNFs-SPE/CNHs/NAF/anti-gltn/BSA biosensors were developed and incubated with 100 pg mL^{-1} of porcine gelatin. ECL intensity was recorded (Fig. 9A), and the corresponding bar graph was plotted (Fig. 9B). The proposed biosensor demonstrated commendable reproducible capability to detect porcine gelatin.

4. Conclusions

In this study, a highly sensitive CNFs-SPE/CNHs/NAF platform was developed for the fabrication of a biosensor to detect porcine gelatin. Interestingly, a carbon nanostructured material-based surface (CNFs-SPE) was modified with another carbon nanostructured material (CNHs) using NAF. Indeed, for the first time, a composite of CNHs/NAF was used to modify CNFs-SPE. Further, the CNHs/NAF nanocomposite-modified CNF-SPE platform exhibited notable capability to enhance the ECL intensity. Moreover, the developed CNFs-SPE/CNHs/NAF/anti-gltn/BSA biosensor demonstrated a wide linear range of 1 pg mL^{-1} to 8 ng mL^{-1} with a detection limit of 1 pg mL^{-1} to detect porcine gelatin. In addition, the CNFs-SPE/CNHs/NAF/anti-gelatin/BSA biosensor demonstrated excellent reproducibility. This developed biosensor has great economic significance in halal industries to be used as an on-site testing device to detect porcine gelatin. However, for the on-site deployment of the developed biosensor for the robust and reliable detection of porcine gelatin, further selectivity, specificity, and potential to detect porcine gelatin in real samples are proposed to be evaluated.[44] Moreover, the CNFs-SPE/CNHs/NAF platform could further be used to develop ECL and electrochemical biosensors for the sensitive detection of different bioanalytes of interest, including ovalbumin and tropomyosin using suitable biorecognition molecules.

Author contributions

Juthi Adhikari: formal analysis, investigation, data curation, and writing – original draft. Mohammad Rizwan: critical revision including writing – review & editing as well as preparation of the article for publication. Minhaz Uddin Ahmed: conceptualization, methodology, validation, resources, data curation, final approval of the version to be published, supervision, project administration, and funding acquisition.

Conflicts of interest

The authors declare no conflict of interest.

Acknowledgements

Minhaz Uddin Ahmed would like to acknowledge the financial support for the project provided by Brunei Research Council (Grant# BRC-10) from the Economic and Planning Development, Prime Minister's Office of Negara Brunei Darussalam. Juthi Adhikari is grateful to the UBD's university graduate scholarship (UGS) for providing the financial support to pursue her Ph.D. degree. Mohammad Rizwan gratefully acknowledges the University of Lodz IDUB grant.

References

1 M. Ali, U. Hashim, S. Mustafa, Y. C. Man, T. S. Dhahi, M. Kashif and S. A. Hamid, Analysis of pork adulteration in commercial meatballs targeting porcine-specific mitochondrial cytochrome b gene by TaqMan probe real-time polymerase chain reaction, *Meat Sci.*, 2012, **91**, 454–459.
2 Y. Demirhan, P. Ulca and H. Z. Senyuva, Detection of porcine DNA in gelatine and gelatine-containing processed food products- Halal/Kosher authentication, *Meat Sci.*, 2012, **90**, 686–689.
3 K. Yue, G. Trujillo-de Santiago, M. M. Alvarez, A. Tamayol, N. Annabi and A. Khademhosseini, Synthesis, properties, and biomedical applications of gelatin methacryloyl (gelma) hydrogels, *Biomaterials*, 2015, **73**, 254–271.
4 S. Galus and J. Kadzińska, Food applications of emulsion-based edible films and coatings, *Trends Food Sci. Technol.*, 2015, **45**, 273–283.
5 H. N. Lubis, N. F. Mohd-Naim, N. N. Alizul and M. U. Ahmed, From market to food plate: Current trusted technology and innovations in halal food analysis, *Trends Food Sci Technol.*, 2016, **58**, 55–68.
6 G. Deng, S. Guo, F. Zaman, T. Li and Y. Huang, Recent advances in animal origin identification of gelatin-based products using liquid chromatography-mass spectrometry methods: A mini review, *Rev. Anal. Chem.*, 2020, **39**, 260–271.
7 J. Biscarat, C. Charmette, J. Sanchez and C. Pochat-Bohatier, Development of a new family of food packaging bioplastics from cross-linked gelatin based films, *Can. J. Chem. Eng.*, 2015, **93**, 176–182.

8 R. M. Lequin, Enzyme immunoassay (EIA)/enzyme-linked immunosorbent assay (ELISA), *Clin. Chem.*, 2005, **51**, 2415–2418.
9 M. Nemati, M. R. Oveisi, H. Abdollahi and O. Sabzevari, Differentiation of bovine and porcine gelatins using principal component analysis, *J. Pharm. Biomed. Anal.*, 2004, **34**, 485–492.
10 G. Zhang, T. Liu, Q. Wang, L. Chen, J. Luo, G. Ma and Z. Su, Mass spectrometric detection of marker peptides in tryptic digests of gelatin: A new method to differentiate between bovine and porcine gelatin, *Food Hydrocolloids*, 2009, **23**, 2001–2007.
11 D. M. Hashim, Y. B. Che Man, R. Norakasha, M. Shuhaimi, Y. Salmah and Z. A. Syahariza, Potential use of Fourier transform infrared spectroscopy for differentiation of bovine and porcine gelatins, *Food Chem.*, 2010, **118**, 856–860.
12 T. Tasara, S. Schumacher and R. Stephan, Conventional and real-time PCR-based approaches for molecular detection and quantification of bovine species material in edible gelatin, *J. Food Prot.*, 2005, **68**, 2420–2426.
13 P. Joshi, R. Mishra and R. J. Narayan, Biosensing applications of carbon-based materials, *Curr. Opin. Biomed. Eng.*, 2021, **18**, 100274.
14 J. Adhikari, M. Rizwan, N. A. Keasberry and M. U. Ahmed, Current progresses and trends in carbon nanomaterials based electrochemical and electrochemiluminescence biosensors, *J. Chin. Chem. Soc.*, 2020, **67**, 1–24.
15 S. A. Lim and M. U. Ahmed, A carbon nanofiber-based label free immunosensor for high sensitive detection of recombinant bovine somatotropin, *Biosens. Bioelectron.*, 2015, **70**, 48–53.
16 M. Rizwan, N. F. Mohd-Naim and M. U. Ahmed, Trends and advances in electrochemiluminescence nanobiosensors, *Sensors*, 2018, **18**, 166.
17 Y. Mei, C. He, W. Zeng, Y. Luo, C. Liu, M. Yang, Y. Kuang, X. Lin and Q. Huang, Electrochemical Biosensors for Foodborne Pathogens Detection Based on Carbon Nanomaterials: Recent Advances and Challenges, *Food Bioprocess Technol.*, 2022, 498–513.
18 M. U. Ahmed, I. Saaem, P. C. Wu and A. S. Brown, Personalized diagnostics and biosensors: a review of the biology and technology needed for personalized medicine, *Crit. Rev. Biotechnol.*, 2014, **34**, 180–196.
19 R. Zhang, K. Fu, F. Zou, H. Bai, G. Zhang, F. Liang and Q. Liu, Highly sensitive electrochemical sensor based on Pt nanoparticles/carbon nanohorns for simultaneous determination of morphine and MDMA in biological samples, *Electrochim. Acta*, 2021, **370**, 137803.
20 Z.-R. Hu, D.-D. Li, T.-H. Kim, M.-S. Kim, T. Xu, M.-G. Ma, S.-E. Choi and C. Si, Lignin-Based/Polypyrrole Carbon Nanofiber Electrode With Enhanced Electrochemical Properties by Electrospun Method, *Front. Chem.*, 2022, DOI: **10.3389/fchem.2022.841956**.
21 S. Zhu and G. Xu, Single-walled carbon nanohorns and their applications, *Nanoscale*, 2010, **2**, 2538–2549.
22 S. Eissa, K. Al-Kattan and M. Zourob, Combination of Carbon Nanofiber-Based Electrochemical Biosensor and Cotton Fiber: A Device for the Detection of the Middle-East Respiratory Syndrome Coronavirus, *ACS Omega*, 2021, **6**, 47.
23 M. Rizwan, N. A. Keasberry and M. U. Ahmed, Efficient double electrochemiluminescence quenching based label-free highly sensitive detection of haptoglobin on a novel nanocomposite modified carbon nanofibers interface, *Sens. Biosensing. Res.*, 2019, **24**, 100284.
24 Q. Wang, Y. Liu, X. Wang, F. Wang, L. Zhang, S. Ge and J. Yu, Ternary Electrochemiluminescence Biosensor Based on DNA Walkers and AuPd Nanomaterials as a Coreaction Accelerator for the detection of miRNA-141, *ACS Appl. Mater. Interfaces*, 2021, **13**, 25783–25791.
25 Y. Cao and J.-J. Zhu, Recent Progress in Electrochemiluminescence of Halide Perovskites, *Front. Chem.*, 2021, **9**, 629830.
26 L. Gutiérrez-Gálvez, T. García-Mendiola, C. Gutiérrez-Sánchez, T. Guerrero-Esteban, C. García-Diego, I. Buendía, M. L. García-Bermejo, F. Pariente and E. Lorenzo, Carbon nanodot-based electrogenerated chemiluminescence biosensor for miRNA-21 detection, *Microchim. Acta*, 2021, **188**, 398.
27 R. Jalili, S. Chenaghlou, A. Khataee, B. Khalilzadeh and M.-R. Rashidi, An Electrochemiluminescence Biosensor for the Detection of Alzheimer's Tau Protein Based on Gold Nanostar Decorated Carbon Nitride Nanosheets, *Molecules*, 2022, **27**, 431.
28 (*a*) N. F. N. Azam, S. Roy, S. A. Lim and M. U. Ahmed, Meat species identification using DNA-luminol interaction and their slow diffusion onto the biochip surface, *Food Chem.*, 2018, **248**, 29–36.
29 M. Rizwan, N. F. Mohd-Naim, N. A. Keasberry and M. U. Ahmed, A highly sensitive and label-free electrochemiluminescence immunosensor for beta 2-microglobulin, *Anal. Methods*, 2017, **9**, 2570–2577.
30 S. Rebeccani, C. Wetzl, V. A. Zamolo, A. Criado, G. Valenti, F. Paoluccia and M. Prato, Electrochemiluminescent immunoassay enhancement driven by carbon nanotubes, *Chem. Commun.*, 2021, **57**, 9672–9675.
31 A. G.-M. Ferrari, S. J. Rowley-Neale and C. E. Banks, Screen-printed electrodes: Transitioning the laboratory in-to-the field, *Talanta Open*, 2021, **3**, 100032.
32 P. Faradillaa, H. Setiyanto, R. V . Manurung and V. Saraswaty, Electrochemical sensor based on screen printed carbon electrode-zinc oxide nano particles/molecularly imprinted-polymer (SPCE–ZnONPs/MIP) for detection of sodium dodecyl sulfate (SDS), *RSC Adv.*, 2022, **12**, 743–752.
33 A. Banerjee, R. K. Calay and F. E. Eregno, Role and Important Properties of a Membrane with Its Recent Advancement in a Microbial Fuel Cell, *Energies*, 2022, **15**, 444.
34 J. Adhikari, M. Rizwan, L. Dennany and M. U. Ahmed, Electrochemiluminescence nanoimmunosensor for CD63 protein using a carbon nanochips/iron oxide/nafion-nanocomposite modified mesoporous carbon interface, *Measurement*, 2021, **170**, 108755.

35 K. Susmitha, M. M. Kumari, A. J. Berkmans, M. N. Kumar, L. Giribabu, S. V. Manorama and M. Raghavender, Carbon nanohorns based counter electrodes developed by spray method for dye sensitized solar cells, *J. Sol. Energy*, 2016, **133**, 524–532.

36 S. Banerjee, M. Sardar, N. Gayathri, A. K. Tyagi and B. Raj, Enhanced conductivity in graphene layers and at their edges, *Appl. Phys. Lett.*, 2006, **88**, 062111.

37 H. N. Yang, D. C. Lee, S. H. Park and W. J. Kim, Preparation of Nafion/various Pt-containing SiO_2 composite membranes sulfonated via different sources of sulfonic group and their application in self-humidifying PEMFC, *J. Membr. Sci.*, 2013, **443**, 210–218.

38 D. Sarkar, D. Mohapatra, S. Ray, S. Bhattacharyya, S. Adak and N. Mitra, Synthesis and characterization of sol-gel derived ZrO_2 doped Al_2O_3 nanopowder, *Ceram. Int.*, 2007, **33**, 1275–1282.

39 Z. Liang, W. Chen, J. Liu, S. Wang, Z. Zhou, W. Li, G. Sun and Q. Xin, FT-IR study of the microstructure of Nafion® membrane, *J. Membr. Sci.*, 2004, **233**, 39–44.

40 J. Davies, C. Thomas, M. Rizwan and C. Gwenin, Development of Electrochemical DNA Biosensor for Equine Hindgut Acidosis Detection, *Sensors*, 2021, **21**, 2319.

41 H. A. G. Hassan-Nixon, N. Singh and A. E. G. Cass, A sensitive impedimetric immunosensor for the detection of Interleukin-8 in nasal epithelial lining fluid of asthma patients, *Biosens. Bioelectron.: X*, 2022, 100118.

42 D. Wu, Y. Liu, Y. Wang, L. Hu, H. Ma, G. Wang and Q. Wei, Label-free Electrochemiluminescent Immunosensor for Detection of Prostate Specific Antigen based on Aminated Graphene Quantum Dots and Carboxyl Graphene Quantum Dots, *Sci. Rep.*, 2016, **6**, 20511.

43 C. Guo, H. Sun and X. S. Zhao, Myoglobin within graphene oxide sheets and Nafion composite films as highly sensitive biosensor, *Sens. Actuators, B*, 2012, **164**, 82–89.

44 S. M. Kamal Uddin, M. A. M. Hossain, S. Sagadevan, M. A. Amin and M. R. Johan, Halal and Kosher gelatin: Applications as well as detection approaches with challenges and prospects, *Food Biosci.*, 2021, **44**, 101422.